Surface Science 606 (2012) 1520–1526

Contents lists available at SciVerse ScienceDirect

Surface Science

journal homepage: www.elsevier.com/locate/susc

Segregation at the surfaces of Cu_xPd_{1-x} alloys in the presence of adsorbed S

James B. Miller [a,b,*], Deepika Priyadarshini [a,b], Andrew J. Gellman [a,b]

[a] National Energy Technology Laboratory-Regional University Alliance (NETL-RUA), US Department of Energy, Pittsburgh, PA 15236, United States
[b] Department of Chemical Engineering, Carnegie Mellon University, Pittsburgh, PA 15213, United States

ARTICLE INFO

Article history:
Received 18 April 2012
Accepted 29 May 2012
Available online 2 June 2012

Keywords:
Surface composition
Surface segregation
Adsorbate induced segregation
PdCu alloys
High throughput
Composition spread alloy films
Hydrogen purification alloys

ABSTRACT

The influence of adsorbed S on surface segregation in Cu_xPd_{1-x} alloys (S/Cu_xPd_{1-x}) was characterized over a wide range of bulk alloy compositions ($x = 0.05$ to 0.95) using high-throughput Composition Spread Alloy Film (CSAF) sample libraries. Top-surface and near-surface compositions of the CSAFs were measured as functions of bulk Cu composition, x, and temperature using spatially resolved low energy ion scattering spectroscopy (LEISS) and X-ray photoemission spectroscopy (XPS). Preferential segregation of Cu to the top-surface of the S/Cu_xPd_{1-x} CSAF was observed at all bulk compositions, x, but the extent of Cu segregation to the S/Cu_xPd_{1-x} surface was lower than the Cu segregation to the surface of a clean Cu_xPd_{1-x} CSAF, clear evidence of an S-induced "segregation reversal." The Langmuir–McLean formulation of the Gibbs isotherm was used to estimate the enthalpy and entropy of Cu segregation to the top-surface, $\Delta H_{seg}(x)$ and $\Delta S_{seg}(x)$, at saturation sulfur coverages. While Cu segregation to the top-surface of the clean Cu_xPd_{1-x} is exothermic ($\Delta H_{seg} < 0$) for all bulk Cu compositions, it is endothermic ($\Delta H_{seg} > 0$) for S/Cu_xPd_{1-x}. Segregation to the S/Cu_xPd_{1-x} surface is driven by entropy. Changes in segregation patterns that occur upon adsorption of S onto Cu_xPd_{1-x} appear to be related to formation of energetically favored Pd–S bonds at the surface, which counterbalance the enthalpic driving forces for Cu segregation to the clean surface.

1. Introduction

The rates and mechanisms of processes that take place on the surfaces of multi-component materials, such as catalysis and corrosion, depend on surface composition. For multi-component materials, surface composition differs from bulk composition because of preferential segregation of one or more components to the surface [1–3]. Surface segregation minimizes the total free energy of the material; it is determined by bulk composition, environmental variables (temperature and pressure) and the presence adsorbed species on the surface [4–6]. An adsorbed species can interact preferentially with one or more of the component materials, resulting in "adsorbate-induced segregation" [7–9]. This phenomenon is of particular importance in the design of catalytic surfaces [10–15]; for example, adsorption of CO is known to induce segregation of Cu to the top surface of Cu–Pt catalysts used for the water–gas shift reaction [10,11,14]. Rational design of complex surface-functional materials for catalysis and other applications requires that segregation be understood, controlled, and even leveraged to achieve optimal material performance. Modern computational tools have contributed to fundamental understanding of segregation phenomena; as an example of particular relevance to this work, Mavrikakis and co-workers have provided a systematic framework, based on first-principle calculations, for understanding adsorbate-induced segregation to the surfaces of alloy catalysts [16–18].

Our interest in segregation follows from our work on Pd-alloys used as membranes for separation of H_2 from mixed gas streams in advanced coal gasification processes [1,2,19–24]. Pure Pd has received significant attention in the separation application because of its surface activity for dissociative adsorption of H_2 and the high diffusivity of H-atoms in its bulk [25–28]. In practice, pure Pd membranes suffer from structural instability in the presence of H_2 [29,30]. Furthermore, exposure of a Pd membrane to H_2S, a common impurity in coal-derived gas streams, degrades membrane performance by poisoning the surface for H_2 dissociation and inhibiting H-atom diffusion through the bulk [22–24,31]. To address these challenges, Pd has been alloyed with a variety of minor components, including Cu, Ag and Au [30,32–37]. CuPd alloys, in particular, have been studied for their resistance to deactivation by H_2S [22–24,31,38].

While the *bulk* composition of a H_2 purification membrane alloy determines the rate of H-atom permeation, the *surface* composition determines the rate of H_2 dissociation. Therefore, the design of a successful separation membrane requires that surface composition be characterized and segregation phenomena be understood. In our previous study of segregation in a clean, polycrystalline $Cu_{0.3}Pd_{0.7}$ alloy, we observed that, when the top-surface, near-surface and bulk are in thermodynamic equilibrium, the top-surface of the alloy is enriched in Cu over a broad range of temperatures [1]. The extent of Cu segregation can be described within the framework of the Langmuir–McLean formulation of the Gibbs isotherm. We also observed that

* Corresponding author at: National Energy Technology Laboratory-Regional University Alliance (NETL-RUA), US Department of Energy, Pittsburgh, PA 15236, United States.
E-mail address: jbmiller@andrew.cmu.edu (J.B. Miller).

0039-6028/$ – see front matter © 2012 Elsevier B.V. All rights reserved.
doi:10.1016/j.susc.2012.05.020

adsorption of S onto the $Cu_{0.3}Pd_{0.7}$ surface suppresses segregation of Cu to the alloy's top-surface [2].

$Cu_{0.3}Pd_{0.7}$ is only one of an infinite number of compositions of CuPd binary alloys. Comprehensive understanding of segregation in an alloy requires its study across the continuum of composition space. Unfortunately, characterization of segregation – or any alloy property – across a broad, continuous composition space can be prohibitively time-consuming when studied using a series of single composition samples. As a consequence, few experimental studies of surface segregation across broad regions of composition space have been reported [3,39,40]. We have extended our study of surface segregation to all of Cu_xPd_{1-x} composition space using a high-throughput approach based on the use of Composition Spread Alloy Film (CSAF) sample libraries [41]. As illustrated in Fig. 1, CSAFs are thin films with continuously variable lateral composition gradients deposited such that every composition of a binary or ternary alloy appears on a compact (~1 cm^2) substrate. When coupled with spatially resolved methods for measuring their composition, structure and functional properties, CSAFs allow rapid characterization of the composition–structure–property relationships that form the basis for rational design of alloys for applications such as H_2 separation.

In our previous high-throughput study of surface segregation on a clean Cu_xPd_{1-x} CSAF, we observed that Cu preferentially segregates to the top-surface of the alloy at all bulk compositions in the range $x = 0.05$ to 0.95 and temperatures in the range T = 300–900 K [41]. We used a Langmuir–McLean analysis to extract ΔH_{seg} and ΔS_{seg}, the enthalpy and entropy of Cu segregation to the alloy top-surface, as functions of bulk composition, x, and showed that Cu segregation is exothermic ($\Delta H_{seg}<0$) over all x [41]. The values of ΔH_{seg} and ΔS_{seg} at $x \sim 0.3$ on the CSAF matched those that we measured for the single composition $Cu_{0.3}Pd_{0.7}$ alloy sample, providing validation of the high throughput approach for characterization of segregation phenomena.

In this work, we use a Cu_xPd_{1-x} CSAF alloy library to assess the influence of adsorbed sulfur on segregation across Cu_xPd_{1-x} composition space. We show that adsorption of sulfur induces segregation reversal, a reduction of the extent of Cu segregation, at all bulk compositions and that, in contrast to the clean alloy in which Cu segregation is exothermic, Cu segregation in the presence of adsorbed S is driven by entropy.

2. Materials and methods

We have described our preparation and characterization of Cu_xPd_{1-x} CSAFs previously [41,42]. Briefly, experiments were carried out in an ultrahigh vacuum chamber with a base pressure of 2×10^{-10} Torr. The chamber is equipped with a monochromated X-ray source (for spatially resolved X-ray photoemission spectroscopy, XPS), a He^+ ion gun (for spatially resolved low energy ion scattering spectroscopy, LEISS), and a sputter gun for substrate cleaning. The CSAF deposition substrate, a 12 mm diameter Mo(110) single crystal (Monocrystals Company), was mounted on a UHV manipulator, in thermal contact with a liquid nitrogen reservoir and with leads for resistive heating to allow temperature control between 80 and 1400 K. After the Mo substrate was mounted in the chamber, carbon was removed from its surface by heating in an O_2 background. The substrate surface was prepared for deposition by cycles of Ar^+ sputtering at 300 K and annealing at 1300 K to reduce other surface impurities to <15 at.%, as measured using XPS.

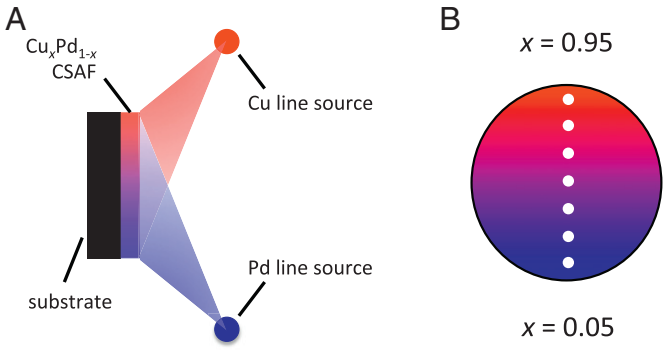

Fig. 1. A) CSAFs are prepared by locating pure component line sources (normal to the plane of the figure) close to, but offset from the centerline of, the substrate. B) A Cu_xPd_{1-x} CSAF contains all compositions (from $x = 0.05$ to 0.95 in this work) on the surface of a compact (12 mm diameter) substrate. Spatially resolved analysis of composition and properties at specific locations on the CSAF (represented by white circles) allows rapid construction of composition–property relationships.

Cu_xPd_{1-x} CSAFs were deposited across the surface of the substrate using an offset filament CSAF deposition tool of our own design that we have described in detail elsewhere [41,42]. Briefly, evaporative line sources for each of the two pure components are positioned offset from the centerline of the substrate to create flux gradients across the substrate surface. As illustrated in Fig. 1, the pure component line sources are positioned parallel to one another, but on opposite sides of the substrate, to create a one-dimensional binary composition gradient across the substrate surface. The flux distribution across the substrate from each line source is controlled by its temperature and the source-substrate geometry [41,42]. Cu and Pd deposition rates across the substrate were calibrated by measuring XPS signal intensities at several substrate locations as functions of time and over a range of source temperatures. The results were used to determine the source temperatures required to give equal deposition rates for each component at the center of the substrate and the deposition times needed to achieve the target CSAF thickness. The bulk composition, x, of the CSAF was calculated at each point on the substrate from the local deposition rates of the two components

$$x = \frac{r_{Cu}\rho_{Cu}}{r_{Cu}\rho_{Cu} + r_{Pd}\rho_{Pd}} \quad (1)$$

where r is the deposition rate of the pure component and ρ is its molar density. A film thickness of ~100 nm was chosen to avoid dewetting from the substrate upon annealing at temperatures through 900 K [41].

XPS measurements were made using a collimated X-ray source (elliptical spot with a 600 μm minor axis along the direction of the composition gradient) to characterize the near-surface composition of the CSAF. All XPS experiments were performed at room temperature at which local composition is stable over the time-scale of the measurement. The Pd $3d_{5/2}$ and Cu $2p_{3/2}$ photoemission intensities (I_{Pd} and I_{Cu}), calibrated against signals from pure component thin films (I^{∞}_{Cu} and I^{∞}_{Pd}), were used to make quantitative estimates of θ^{ns}_{Cu}, the Cu atom fraction in the near surface region (~7 atomic layers):

$$\theta^{ns}_{Cu} = \frac{I_{Cu}/I^{\infty}_{Cu}}{(I_{Cu}/I^{\infty}_{Cu}) + (I_{Pd}/I^{\infty}_{Pd})}. \quad (2)$$

LEISS experiments using a He^+ ion beam with ~800 μm spot diameter and $E_0 = 750$ eV were performed to measure θ^{top}_{Cu}, the top-surface (the topmost atomic layer) composition of the CSAF. Quantitative estimates of the top-surface composition were made by comparing the intensities of Cu (at $E/E_0 \sim 0.89$) and Pd (at $E/E_0 \sim 0.93$) scattering features to those measured on pure component films.

Annealed CSAFs were exposed to H_2S at 300 K by backfilling the UHV chamber to 10^{-8} Torr with H_2S (Matheson, 99.995%) for controlled time intervals. Exposures are expressed in units of Langmuir (L); $1\ L = 10^{-6}$ Torr·sec. After exposure, adsorbed H_2S was decomposed to atomic S, with liberation of H_2, by heating to 400 K [2].

3. Results

3.1. S adsorption onto the Cu_xPd_{1-x} CSAF

The H_2S exposure conditions required to saturate the CSAF with adsorbed S were determined by exposing pure Pd and Cu films to increasing amounts of H_2S. Pure component films were formed by deposition of Pd or Cu onto the Mo(110) substrate until the XPS signal of the Mo substrate was no longer detectable. Our previous work with S deposition from H_2S onto a bulk polycrystalline $Cu_{0.3}Pd_{0.7}$ alloy demonstrated that thermally induced decomposition of adsorbed H_2S is complete by 400 K [2]. Therefore, the pure metal films were exposed to increasing amounts of H_2S at 300 K and then annealed at 400 K to decompose the H_2S. Fig. 2 shows the S 2p XPS signals as functions of H_2S exposure for the pure Pd and Cu films. The S 2p XPS signals saturate after exposures of 0.5 L on the Pd film and 1 L on the Cu film. Therefore, an H_2S exposure of 2 L was used to ensure saturation coverage of S on the Cu_xPd_{1-x} CSAF. The absolute S photoemission signal at saturation coverage differs for the two pure component films; the signal from S on Cu is about 86% of the S on Pd signal (570 versus 660 cps). We will address this observation in the Discussion section.

3.2. S content of the S/Cu_xPd_{1-x} CSAF surface

Fig. 3 displays the S 2p XPS signal as a function of bulk alloy composition, x, measured at 300 K after annealing the S/Cu_xPd_{1-x} CSAF for 20 min at temperatures in the range 300–800 K. Two primary trends are apparent. First, at bulk compositions through $x \sim 0.85$ the S photoemission signal does not vary significantly with x. At higher values of x (the Cu-rich region of the CSAF) the S signal falls significantly. At 300 K, for example, the S 2p photoemission signal at the highest value of x is ~77% of the S 2p signal at the lowest value of x. This result is consistent with results from the pure component saturation experiments described in Section 3.1, in which the S 2p photoemission signal from the S saturated Cu film was ~86% of that measured on the S saturated Pd film.

The second trend observed in Fig. 3 is that, upon annealing at 700 and 800 K, the S signal decreases at all values of x. In our previous study of $S/Cu_{0.3}Pd_{0.7}$, we observed that S does not desorb from the alloy surface during heating to 900 K [2]; therefore, it is unlikely that the decreases in S photoemission that we report here are a result of S desorption. Instead, upon annealing at 700 and 800 K, S diffuses into the near-surface of the CSAF.

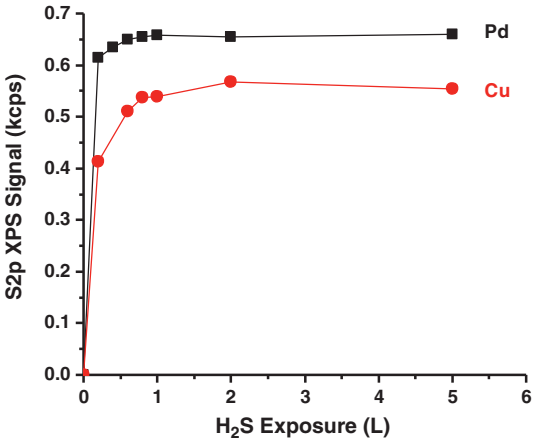

Fig. 2. S 2p XPS signal as a function of H_2S exposure for pure Pd and Cu films. Exposures were performed at 300 K, followed by heating to 400 K to induce H_2S decomposition.

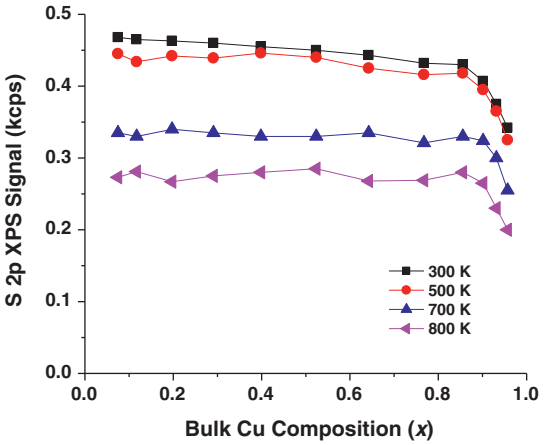

Fig. 3. S 2p XPS signal as a function of anneal temperature and bulk Cu composition of the S-exposed Cu_xPd_{1-x} CSAF. The S signal on the Pd-rich side (low x) is greater than on the Cu-rich (high x) side. Upon annealing, the S signal decreases at all bulk compositions.

3.3. Cu and Pd contents of the CSAF surface

A 100 nm thick Cu_xPd_{1-x} CSAF was prepared by co-depositing opposing Cu and Pd gradients onto the Mo(110) substrate at 300 K. We previously showed that the near-surface compositions (from XPS) of clean, 100 nm Cu_xPd_{1-x} CSAFs are stable after annealing for 15 min at 700 K or above [41]; in this work, the as-deposited film was equilibrated by annealing at 900 K for 20 min. The near-surface composition, θ_{Cu}^{ns}, of the clean, equilibrated film was measured at 300 K at several locations (bulk compositions, x) on the CSAF surface while its top-surface (LEISS) composition, θ_{Cu}^{top}, was measured at 900 K. Values of θ_{Cu}^{ns} and θ_{Cu}^{top} for the clean (before H_2S exposure) surface are plotted versus bulk composition as open, black squares in Fig. 4. The near-surface composition shown in Fig. 4A is approximately equal to the bulk composition over the entire bulk composition range, but with slight Cu depletion (Pd enrichment), especially at high bulk Cu composition. The top-surface is, on the other hand, enriched in Cu at all bulk compositions (Fig. 4B); the degree of Cu enrichment is especially high at mid-range bulk compositions. As an example of typical segregation patterns on the clean Cu_xPd_{1-x} CSAF surface, at $x = 0.52$, $\theta_{Cu}^{ns} = 0.49$ and $\theta_{Cu}^{top} = 0.74$. Our observation of top-surface Cu enrichment at the expense of near-surface Cu content matches results that we reported for a single-composition, polycrystalline $Cu_{0.3}Pd_{0.7}$ [1]. Within experimental uncertainty, the segregation patterns shown here for the clean CSAF are the same as those reported in our prior study of segregation at the surface of a clean Cu_xPd_{1-x} CSAF [41].

The clean, equilibrated Cu_xPd_{1-x} CSAF was then exposed to 2 L of H_2S at 300 K; H_2S was subsequently decomposed at 400 K to generate the saturation coverage of adsorbed S. The S-treated CSAF was then cooled to 300 K where XPS was used to determine θ_{Cu}^{ns}. The CSAF was then annealed for 20 min at 500, 700 and 900 K. After annealing at each temperature, θ_{Cu}^{ns} was measured at 300 K using XPS. Fig. 4A shows that the presence of adsorbed S induces slight depletion of Cu (Pd enrichment) in the near-surface; for example, at $x = 0.52$ S adsorption followed by annealing at 300 K reduces θ_{Cu}^{ns} from 0.49 to 0.45. As the S/Cu_xPd_{1-x} CSAF is annealed at higher temperatures, the extent of Cu depletion decreases; after annealing at 900 K, the near-surface composition is nearly the same as it was on the clean, equilibrated Cu_xPd_{1-x} CSAF. The magnitudes of the changes in the near-surface Cu composition are roughly equivalent to the uncertainty of the XPS composition measurements; however, the trends are reproducible across replicate experiments.

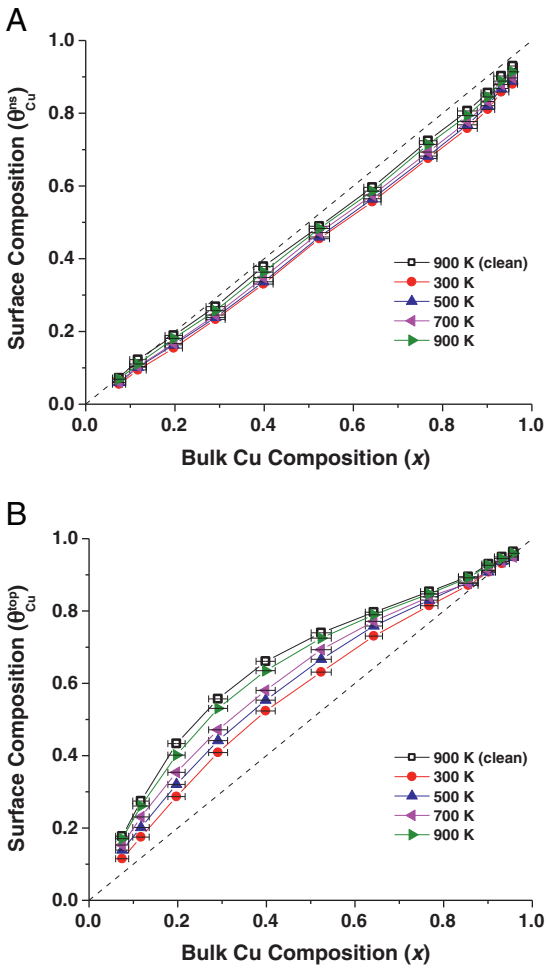

Fig. 4. A) Near-surface and B) top-surface compositions of a 100 nm thick Cu_xPd_{1-x} CSAF exposed to H_2S. The near-surface compositions were measured using XPS at 300 K after annealing the film at the indicated temperature for 20 min; the top-surface compositions were measured using LEISS at the indicated temperature, but after first annealing at 900 K. The surface compositions of the clean Cu_xPd_{1-x} CSAF after annealing at 900 K are shown as open black squares.

Fig. 4B shows the top-surface compositions (from LEISS) of the S/Cu_xPd_{1-x} CSAF, measured after the 900 K anneal, at temperatures in the range 300 to 900 K as functions of x. Our choice to perform LEISS experiments on the S/Cu_xPd_{1-x} CSAF *after* first annealing the sample at the highest temperature used for LEISS (900 K) ensures that the S coverage remained constant during the measurements of θ_{Cu}^{top} at lower temperatures. Measured top-surface compositions are reversible: at every bulk composition and temperature, the measured composition is the same whether approached from high or low temperatures. At all temperatures and all bulk compositions, the top-surface is enriched in Cu, i.e. $\theta_{Cu}^{top} > x$. However, as shown in Fig. 5, θ_{Cu}^{top} at the S/Cu_xPd_{1-x} surface is always *less* than at the clean Cu_xPd_{1-x} surface at the same bulk composition and temperature. In other words, the presence of adsorbed S *reduces* the extent of Cu segregation to the top surface, providing clear evidence of *adsorption induced segregation reversal*. As S/Cu_xPd_{1-x} is heated from 300 through 900 K, θ_{Cu}^{top} increases and approaches that of the clean, sample equilibrated at 900 K. This behavior differs from that of a clean Cu_xPd_{1-x} CSAF surface, for which θ_{Cu}^{top} exhibits a reversible maximum at 700 K [41]. The fact that Cu segregation increases monotonically with temperature on the S/Cu_xPd_{1-x} CSAF is suggestive of an entropically driven segregation process [5]; we will return to this point in the Discussion section.

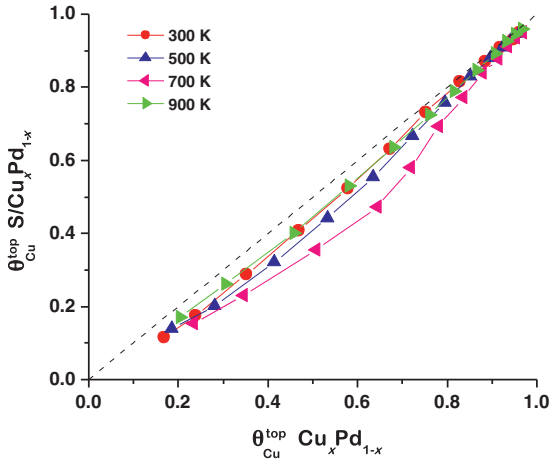

Fig. 5. Comparison of the top-surface Cu compositions of S/Cu_xPd_{1-x} and clean Cu_xPd_{1-x}. At all bulk compositions and temperatures, the top-surface Cu content of S/Cu_xPd_{1-x} is lower than that of clean Cu_xPd_{1-x}, illustrating that adsorbed S induces a Cu segregation reversal.

4. Discussion

4.1. Segregation in $S/Cu_{0.3}Pd_{0.7}$ and S/Cu_xPd_{1-x} CSAF at $x = 0.3$

The top-surface layer of the S/Cu_xPd_{1-x} CSAF, while enriched in Cu, clearly contains both Pd and Cu atoms (Fig. 4B). In our earlier work with polycrystalline $Cu_{0.3}Pd_{0.7}$, we observed that the S-treated surface contained only Pd and S atoms—Cu was notably absent [2]. The difference between the results of the experiment on polycrystalline $Cu_{0.3}Pd_{0.7}$ and the ones reported here arises from differences in surface preparation prior to H_2S exposure. In the current work, a thoroughly annealed (at 900 K) Cu_xPd_{1-x} CSAF, with its top-surface enriched in Cu, was exposed to H_2S. In the original work with $Cu_{0.3}Pd_{0.7}$, H_2S was exposed to a surface prepared by Ar^+ sputtering but with no subsequent annealing.

To confirm the effect of surface preparation on segregation patterns at S-modified Cu_xPd_{1-x} surfaces, we exposed the $Cu_{0.3}Pd_{0.7}$ sample used in the previous study to H_2S using the same procedure we used for the Cu_xPd_{1-x} CSAF. The $Cu_{0.3}Pd_{0.7}$ sample was annealed at 900 K before H_2S exposure and then annealed again at 900 K before making LEISS measurements at temperatures in the range 300–900 K. The top-surface Cu composition of the $S/Cu_{0.3}Pd_{0.7}$ alloy is plotted as a function of temperature in Fig. 6 (black squares). The values of θ_{Cu}^{top} on $S/Cu_{0.3}Pd_{0.7}$ are in excellent agreement with those at x ~0.3 on the S/Cu_xPd_{1-x} CSAF (red circles, replotted from Fig. 4B), providing another demonstration of the appropriateness of the CSAF platform for the study of surface segregation. Furthermore, these results confirm that sputtering does indeed change the nature of H_2S' interaction with the alloy surface and its impact on segregation. The high defect density and low surface Cu concentration of the sputtered surface (sputtering preferentially removes Cu atoms) likely change its interaction with H_2S. This interesting observation, which is beyond the scope of this paper, is deserving of continued investigation.

4.2. S-uptake by the Cu_xPd_{1-x} CSAF

Using electron backscatter diffraction, we previously showed that annealing Cu_xPd_{1-x} CSAFs prepared on Mo(110) at 800 K results in formation of local bulk structures consistent with the CuPd phase diagram [41,43]. In regions with purely FCC order ($x<0.51$ and $x>0.68$), we observed that grains are oriented such that they expose predominantly the (111) plane of the FCC lattice. At 900 K, the bulk CuPd phase diagram displays FCC order at all compositions [43]; thus, it is reasonable to assume that the CSAFs studied in this work

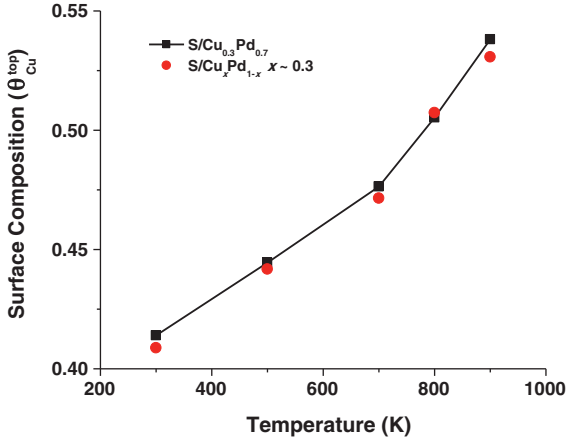

Fig. 6. Top-surface composition of $S/Cu_{0.30}Pd_{0.70}$ as a function of temperature (black squares). The clean $Cu_{0.30}Pd_{0.70}$ alloy was annealed at 900 K, then exposed to 2 L H_2S at 300 K and finally annealed at 400 K to induce H_2S decomposition. The surface composition was measured at temperature using LEISS. Top-surface compositions measured on a comparably prepared S/Cu_xPd_{1-x} CSAF at $x \sim 0.3$ (red circles, from Fig. 4(b)) are shown for comparison.

present primarily FCC(111) facets at all bulk compositions, x. Because the lattice parameter of Cu (0.361 nm) is smaller than that of Pd (0.389 nm), the *areal* density of S atoms for any given S-overlayer configuration would be higher on a Cu(111) surface than on a Pd(111) surface, with a correspondingly higher raw S photoemission signal. Clearly, this is not the case in the present work; the S 2p photoemission signals from S-saturated pure Cu film (Fig. 2) and from the Cu-rich end of the Cu_xPd_{1-x} CSAF (Fig. 3) are both significantly *lower* than the S 2p signals from the S-saturated pure Pd film and the Pd-rich end of the Cu_xPd_{1-x} CSAF.

The composition dependence of S-uptake may reflect differences in the local ordering of S atoms on $Cu_xPd_{1-x}(111)$ facets. While we have not collected direct evidence for formation of ordered S-overlayers on the surfaces of the samples described here, studies of S-modified Pd(111) (including our own [44,45]) and Cu(111) single crystal surfaces provide context for our results. At 300 K, exposure of Pd(111) to H_2S or S_2 typically results in the formation of a Pd(111)-$\left(\sqrt{3}\times\sqrt{3}\right)$R30-S (herein "$\sqrt{3}$") structure [44–49]. In the $\sqrt{3}$ configuration, S atoms are bound in three-fold hollow surface sites without subsurface occupancy. At temperatures above 400 K, a complex Pd(111)-$\left(\sqrt{7}\times\sqrt{7}\right)$R19-S (herein "$\sqrt{7}$") overlayer forms [44–46,48,49]. In the $\sqrt{7}$ structure, S atoms reside at both top-surface and subsurface locations [44,45]; the $\sqrt{7}$ structure is sometimes viewed as an early stage of penetration of surface S atoms into the Pd bulk. Cu(111) displays a different behavior upon room temperature exposure to H_2S: the $\sqrt{7}$ S overlayer forms directly, without the appearancez of a $\sqrt{3}$ structure [50–52].

It is plausible that different S-overlayers form at different locations (i.e., bulk compositions, x) on the CSAF surface. Some of the S atoms deposited by H_2S decomposition onto the Cu-rich side of the CSAF and the pure Cu film may reside at subsurface locations, as they do in Cu(111)-$\sqrt{7}$; S atoms deposited by H_2S decomposition onto the pure Pd film and on the CSAF at $x<0.85$ may reside exclusively at the top-layer, as they do on Pd(111)-$\sqrt{3}$. The difference between the two overlayer structures is important because subsurface S atoms, such as those in the $\sqrt{7}$ structure, contribute significantly less to the total S 2p photoemission signal than S atoms at the top-surface. Thus, in this scenario, S 2p photoemission is expected to be lower at Cu-rich compositions, which is precisely the pattern that we observe in both the single component films (Fig. 2) and the CSAF (Fig. 3).

Upon post-deposition annealing at elevated temperatures, both top-surface and subsurface S atoms diffuse from their initial locations into the interior of the CSAF, resulting in a reduction of S 2p photoemission intensity at all bulk compositions across the CSAF, as shown in Fig. 3.

4.3. Estimation of ΔH_{seg} and ΔS_{seg}

The thermodynamics of surface segregation can be characterized by the Langmuir–McLean formulation of the Gibbs isotherm: [4,5,53,54]

$$\begin{aligned}\frac{\theta_{Cu}^{top}}{\theta_{Pd}^{top}} &= \frac{x_{Cu}^{bulk}}{x_{Pd}^{bulk}}\exp\left(\frac{-\Delta G_{seg}}{RT}\right)\\ \frac{\theta_{Cu}^{top}}{\left(1-\theta_{Cu}^{top}\right)} &= \frac{x}{(1-x)}\exp\left(\frac{-\Delta G_{seg}}{RT}\right)\\ \frac{\theta_{Cu}^{top}}{\left(1-\theta_{Cu}^{top}\right)} &= \frac{x}{(1-x)}\exp\left(\frac{-\Delta H_{seg}}{RT}+\frac{\Delta S_{seg}}{R}\right).\end{aligned} \quad (3)$$

The thermodynamic parameters ΔG_{seg}, ΔH_{seg}, and ΔS_{seg} are the free energy, enthalpy and entropy of Cu segregation to the top-surface of the alloy. We previously used the Langmuir–McLean equation to extract ΔH_{seg} and ΔS_{seg} for segregation of Cu to the top-most layer of a clean Cu_xPd_{1-x} CSAF as functions of bulk composition, x. As noted earlier, the enthalpies and entropies of segregation on the clean CSAF at $x=0.3$ compared well with those from $Cu_{0.3}Pd_{0.7}$ [41].

We performed a Langmuir–McLean analysis of the temperature dependent top-surface Cu compositions shown in Fig. 4B to estimate ΔH_{seg} and ΔS_{seg} for the S/Cu_xPd_{1-x} surface. As for the clean Cu_xPd_{1-x} CSAF, we fit the Langmuir–McLean equation to surface composition data obtained at 700 K and above, where the bulk, near-surface and top-surface compositions are in thermodynamic equilibrium [41]. Values of ΔH_{seg} and $T\Delta S_{seg}$ (at $T=800$ K) for both the clean (reproduced from [41]) and S covered surface are plotted in Fig. 7 as functions of bulk Cu composition. The most significant difference between the clean and S-covered Cu_xPd_{1-x} surfaces is that Cu segregation to the clean surface is exothermic ($\Delta H_{seg}<0$) for all values of x, while Cu segregation to the S/Cu_xPd_{1-x} surface is endothermic ($\Delta H_{seg}>0$). This difference can be explained in terms of the energetics of surface sulfide formation [7–9]. The enthalpies of formation of bulk CuS and PdS are −53.1 and −75 kJ/mol, respectively [55]. Enthalpies of S adsorption onto metal surfaces correlate with bulk heats of bulk sulfide formation [56,57], thus we expect adsorption of S onto Pd to be energetically favored over adsorption onto Cu. Formation of energetically favored Pd–S bonds at the CSAF surface counterbalances, at least in part, the enthalpic driver for Cu segregation to the top-surface.

In spite of being endothermic, Cu segregation to the S/Cu_xPd_{1-x} top-surface occurs – but, as shown in Fig. 5, to a lesser extent than for the clean Cu_xPd_{1-x} surface – because of entropy changes that favor segregation. For S/Cu_xPd_{1-x}, $T\Delta S_{seg}$ is significantly larger than it is for clean Cu_xPd_{1-x}. In fact, $T\Delta S_{seg}$ is large enough to overcome the positive value of ΔH_{seg} and result in a net free energy *decrease* for Cu segregation to the S/Cu_xPd_{1-x} surface over all x. A complete atomic-level description of the processes that contribute to entropy changes that occur upon segregation to the S/Cu_xPd_{1-x} surface is beyond the scope of this study. However, we make two observations that frame the issue. First, the standard entropies of formation of CuS and PdS are 1.2 and −23.7 J/mol K (calculated from properties tabulated in [55]), allowing us to rule out formation of Pd–S bonds as the driver of the large entropy increase that accompanies segregation. Second, in the absence of an explanation based on chemical bond formation, we note that the entropy increase may reflect local

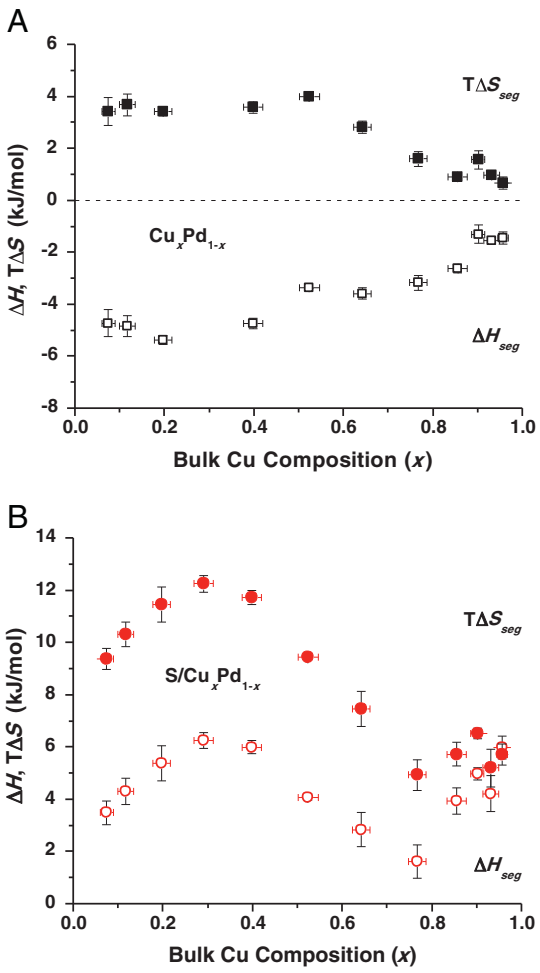

Fig. 7. ΔH_{seg} and $T\Delta S_{seg}$ (at 800 K) as functions of bulk composition for A) clean Cu_xPd_{1-x} and B) S/Cu_xPd_{1-x} CSAFs. Cu segregation to the top-surface is exothermic for the clean Cu_xPd_{1-x} CSAF, but endothermic for S/Cu_xPd_{1-x}. For the clean Cu_xPd_{1-x} CSAF, enthalpic and entropic effects both contribute to Cu segregation; entropy drives segregation in the S/Cu_xPd_{1-x} case.

disordering of the surface – perhaps disruption of S-overlayers – that occurs as Cu atoms segregate to the top-surface [5]. Clearly this is an interesting subject that is worthy of additional investigation.

Fig. 7 also shows that, as functions of x, both ΔH_{seg} and ΔS_{seg} for S/Cu_xPd_{1-x} exhibit clear discontinuities near $x \sim 0.8$. This is nearly the same composition at which a discontinuity in S-photoemission intensity from S/Cu_xPd_{1-x} was observed (Fig. 3). The discontinuities in the thermodynamic parameters are likely another reflection of changes in the structure of the sulfide overlayers that occur with composition.

5. Conclusions

A high throughput methodology, based on the use of CSAF alloy libraries, was applied to the study of segregation to the surface of Cu_xPd_{1-x} alloys for x from 0.05 to 0.95 and in the presence of adsorbed sulfur. Significantly, the results of segregation measurements performed on the Cu_xPd_{1-x} CSAF at $x \sim 0.3$ match those made for a bulk, polycrystalline $Cu_{0.3}Pd_{0.7}$ alloy, demonstrating the utility of the CSAF platform for characterization of segregation phenomena. Cu segregates to the surface of the Cu_xPd_{1-x} alloy in the presence of adsorbed sulfur, but to a lesser extent than it does in the case of a clean Cu_xPd_{1-x} alloy surface: S induces segregation reversal. Cu segregation, which is exothermic for the clean surface, becomes endothermic in the presence of adsorbed sulfur; formation of thermodynamically favored Pd–S bonds at the alloy surface counterbalances the enthalpic driving force for Cu segregation. In the presence of sulfur, Cu segregation is driven by entropy changes.

Disclaimer

This project was funded, in part, by the Department of Energy, National Energy Technology Laboratory, an agency of the United States Government, through a support contract with URS Energy & Construction, Inc. Neither the United States Government nor any agency thereof, nor any of their employees, nor URS Energy & Construction, Inc., nor any of their employees, makes any warranty, expressed or implied, or assumes any legal liability or responsibility for the accuracy, completeness, or usefulness of any information, apparatus, product, or process disclosed, or represents that its use would not infringe privately owned rights. Reference herein to any specific commercial product, process, or service by trade name, trademark, manufacturer, or otherwise, does not necessarily constitute or imply its endorsement, recommendation, or favoring by the United States Government or any agency thereof. The views and opinions of authors expressed herein do not necessarily state or reflect those of the United States Government or any agency thereof.

Acknowledgements

As part of the National Energy Technology Laboratory's Regional University Alliance (NETL-RUA), a collaborative initiative of the NETL, this technical effort was performed under the RES contract DE-FE0004000. This work was supported by the National Science Foundation (CBET 1033804).

References

[1] J.B. Miller, C. Matranga, A.J. Gellman, Surf. Sci. 602 (2008) 375.
[2] J.B. Miller, B.D. Morreale, A.J. Gellman, Surf. Sci. 602 (2008) 1819.
[3] C.W. Yi, K. Luo, T. Wei, D.W. Goodman, J. Phys. Chem. B 109 (2005) 18535.
[4] S. Hoffmann, in: P.A. Doben, A. Miller (Eds.), Surface Segregation Phenomena, CRC Press, CRC Press, Boston, 1990, p. 110.
[5] M. Polak, L. Rubinovich, Surf. Sci. Rep. 38 (2000) 127.
[6] G.A. Somorjai, Introduction to Surface Chemistry and Catalysis, Wiley, 1994.
[7] S. Modak, B. Khanra, Phys. Chem. Lett. 134 (1987) 39.
[8] D. Tomanek, S. Mukherjee, V. Kumar, K.H. Bennemann, Surf. Sci. 114 (1982) 11.
[9] W. Unger, S. Baunack, Surf. Sci. 184 (1987) L361.
[10] K.J. Andersson, F. Calle-Vallejo, J. Rossmeisl, I. Chorkendorff, J. Am. Chem. Soc. 131 (2009) 2404.
[11] K.J. Andersson, I. Chorkendorff, Surf. Sci. 604 (2010) 1733.
[12] W. Chen, P. Dalach, W.F. Schneider, C. Wolverton, Langmuir 28 (2012) 4683.
[13] F. Gao, Y. Wang, D.W. Goodman, J. Phys. Chem. C 113 (2009) 14993.
[14] J. Knudsen, A.U. Nilekar, R.T. Yang, J. Schnadt, E.L. Kunkes, J.A. Dumesic, M. Mavrikakis, F. Besenbacher, J. Am. Chem. Soc. 129 (2007) 6485.
[15] O.M. Lovvik, S.M. Opalka, Surf. Sci. 602 (2008) 2840.
[16] J. Greeley, M. Mavrikakis, Nat. Mater. 3 (2004) 810.
[17] J. Greeley, M. Mavrikakis, Catal. Today 111 (2006) 52.
[18] A.U. Nilekar, A.V. Ruban, M. Mavrikakis, Surf. Sci. 603 (2009) 91.
[19] M.L. Bosko, J.B. Miller, E.A. Lombardo, A.J. Gellman, L.M. Cornaglia, J. Membr. Sci. 369 (2011) 267.
[20] W.D. Michalak, J.B. Miller, D.R. Alfonso, A.J. Gellman, Surf. Sci. 606 (2012) 146.
[21] J.B. Miller, D.R. Alfonso, B.H. Howard, C.P. O'Brien, B.D. Morreale, J. Phys. Chem. C 113 (2009) 18800.
[22] C.P. O'Brien, A.J. Gellman, B.D. Morreale, J.B. Miller, J. Membr. Sci. 371 (2011) 263.
[23] C.P. O'Brien, B.H. Howard, J.B. Miller, B.D. Morreale, A.J. Gellman, J. Membr. Sci. 349 (2010) 380.
[24] C.P. O'Brien, J.B. Miller, B.D. Morreale, A.J. Gellman, J. Phys. Chem. C 115 (2011) 24221.
[25] R.E. Buxbaum, T.L. Marker, J. Membr. Sci. 85 (1993) 29.
[26] F.A. Lewis, The Palladium–Hydrogen System, Academic Press, New York, 1967.
[27] S.N. Paglieri, J.D. Way, Sep. Purif. Methods 31 (2002) 1.
[28] B.D. Morreale, M.V. Ciocco, R.M. Enick, B.I. Morsi, B.H. Howard, A.V. Cugini, K.S. Rothenberger, J. Membr. Sci. 212 (2003) 87.
[29] H.C. Rogers, Science 159 (1968) 1057.
[30] S. Yun, S.T. Oyama, J. Membr. Sci. 375 (2011) 28.
[31] B.D. Morreale, The influence of H2S on palladium and palladium–copper alloy membranes, Chemical Engineering, University of Pittsburgh, 2006.
[32] C. Ling, L. Semidey-Flecha, D.S. Sholl, J. Membr. Sci. 371 (2011) 189.
[33] Y. Sakamoto, K. Yuwasa, K. Hirayama, J. Less-Common Met. 88 (1992) 115.
[34] D.S. Sholl, J. Alloys Compd. 446 (2007) 462.

[35] D.S. Sholl, Y.H. Ma, MRS Bull. 31 (2006) 770.
[36] N.I. Timofeev, F.N. Berseneva, V.I. Gromov, Mater. Sci. 17 (1982) 417.
[37] H. Yoshida, K. Okuno, Y. Naruse, T. Kashiwai, Fusion Technol. 8 (1985) 2388.
[38] B.H. Howard, R.P. Killmeyer, K.S. Rothenberger, A.V. Cugini, B.D. Morreale, R.M. Enick, F. Bustamante, J. Membr. Sci. 241 (2004) 207.
[39] W. Losch, J. Vac. Sci. Technol. 15 (1978) 1541.
[40] P. Laty, J.C. Joud, P. Desre, Surf. Sci. 104 (1981) 105.
[41] D. Priyadarshini, P. Kondratyuk, Y.N. Picard, B.D. Morreale, A.J. Gellman, J.B. Miller, J. Phys. Chem. C 115 (2011) 10155.
[42] D. Priyadarshini, P. Kondratyuk, J.B. Miller, A.J. Gellman, J. Vac. Sci. Technol., A 30 (2012).
[43] P.R. Subramanian, D.E. Laughlin, Cu–Pd (copper–palladium), in: T.B. Massalski (Ed.), Binary Alloy Phase Diagrams, ASM International, 1990, p. 1454.
[44] J.G. Forbes, A.J. Gellman, J.C. Dunphy, M. Salmeron, Surf. Sci. 279 (1992) 68.
[45] J.B. Miller, A.J. Gellman, Surf. Sci. 603 (2009) L82.
[46] M.E. Grillo, C. Stampfl, W. Berndt, Surf. Sci. 317 (1994) 84.
[47] F. Maca, M. Scheffler, W. Berndt, Surf. Sci. 160 (1985) 467.
[48] C.H. Patterson, R.M. Lambert, Surf. Sci. 187 (1987) 339.
[49] S. Speller, T. Rauch, J. Bromermann, P. Borrmann, W. Heiland, Surf. Sci. 441 (1999) 107.
[50] C.T. Campbell, B.E. Koel, Surf. Sci. 183 (1987) 100.
[51] G.J. Jackson, S.M. Driver, D.P. Woodruff, B.C.C. Cowie, R.G. Jones, Surf. Sci. 453 (2000) 183.
[52] N.P. Prince, D.L. Seymour, M.J. Ashwin, C.F. McConville, D.P. Woodruff, R.G. Jones, Surf. Sci. 230 (1990) 13.
[53] F.F. Abraham, C.R. Brundle, J. Vac. Sci. Technol. 18 (1981) 506.
[54] P. Wynblatt, R.C. Ku, Surf. Sci. 65 (1977) 511.
[55] Standard thermodynamic properties of chemical substances, in: D.R. Lide (Ed.), CRC Handbook of Chemistry and Physics, Taylor and Francis, 2008.
[56] J. Benard, J. Oudar, N. Barbouth, E. Margot, Y. Berthier, Surf. Sci. 88 (1979) L35.
[57] J. Oudar, Catal. Rev. Sci. Eng. 22 (1980) 171.